



HAL
open science

Insight into Organometallic Intermediate and Its Evolution to Covalent Bonding in Surface-Confined Ullmann Polymerization

Marco Di Giovannantonio, Mohamed El Garah, Josh Lipton-Duffin, Vincent Meunier, Luis Cardenas, Yannick Fagot-Révurat, Albano Cossaro, Alberto Verdini, Dmitrii F. Perepichka, Federico Rosei, et al.

► To cite this version:

Marco Di Giovannantonio, Mohamed El Garah, Josh Lipton-Duffin, Vincent Meunier, Luis Cardenas, et al.. Insight into Organometallic Intermediate and Its Evolution to Covalent Bonding in Surface-Confined Ullmann Polymerization. *ACS Nano*, 2013, 7 (9), pp.8190-8198. 10.1021/nn4035684 . hal-01273653

HAL Id: hal-01273653

<https://hal.science/hal-01273653v1>

Submitted on 18 Jun 2024

HAL is a multi-disciplinary open access archive for the deposit and dissemination of scientific research documents, whether they are published or not. The documents may come from teaching and research institutions in France or abroad, or from public or private research centers.

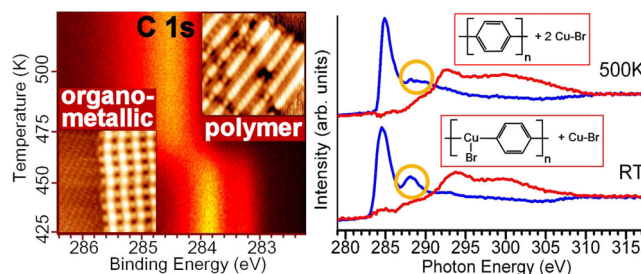
L'archive ouverte pluridisciplinaire **HAL**, est destinée au dépôt et à la diffusion de documents scientifiques de niveau recherche, publiés ou non, émanant des établissements d'enseignement et de recherche français ou étrangers, des laboratoires publics ou privés.

Insight into Organometallic Intermediate and Its Evolution to Covalent Bonding in Surface-Confined Ullmann Polymerization

Marco Di Giovannantonio,[†] Mohamed El Garah,[‡] Josh Lipton-Duffin,[‡] Vincent Meunier,[§] Luis Cardenas,[‡] Yannick Fagot Revurat,[⊥] Albano Cossaro,^{||} Alberto Verdini,^{||} Dmitrii F. Perepichka,^{#,*} Federico Rosei,^{#,*,*} and Giorgio Contini^{†,∇,*}

[†]Istituto di Struttura della Materia, CNR, Via Fosso del Cavaliere 100, 00133 Roma, Italy, [‡]Centre Énergie, Matériaux et Télécommunications, Institut National de la Recherche Scientifique, 1650 Boulevard Lionel-Boulet, Varennes, QC J3X 1S2, Canada, [§]Department of Physics, Applied Physics, and Astronomy, Rensselaer Polytechnic Institute, 110 8th Street, Troy, New York 12180, United States, [⊥]Institut Jean Lamour, UMR 7198, Université Lorraine/CNRS, B.P. 239 FE-54506, Vandoeuvre-les-Nancy, France, ^{||}IOM-CNR, Laboratorio TASC, 34149 Trieste, Italy, [#]Department of Chemistry and Centre for Self-Assembled Chemical Structures, McGill University, 801 Sherbrooke Street West, Montreal, QC H3A 2K6, Canada, and [∇]Department of Physics and Centro Interdipartimentale Nanoscienze & Nanotecnologie & Strumentazione (NAST), University of Rome "Tor Vergata", 00133 Roma, Italy

ABSTRACT We provide insight into surface-catalyzed dehalogenative polymerization, analyzing the organometallic intermediate and its evolution into planar polymeric structures. A combined study using scanning tunneling microscopy (STM), X-ray photoelectron spectroscopy (XPS), low energy electron diffraction (LEED), near-edge X-ray absorption fine structure (NEXAFS) spectroscopy and first-principles calculations unveils the structural conformation of substrate-bound phenylene intermediates generated from 1,4-dibromobenzene precursors on Cu(110), showing the stabilizing role of the halogen. The appearance of covalently bonded conjugated structures is followed in real time by fast-XPS measurements (with an acquisition time of 2 s per spectrum and heating rate of 2 K/s), showing that the detaching of phenylene units from the copper substrate and subsequent polymerization occur upon annealing above 460 ± 10 K.



KEYWORDS: conjugated polymers · surface polymerization · Ullmann coupling · poly(*para*-phenylene) (PPP) · scanning tunneling microscopy (STM) · fast X-ray photoelectron spectroscopy (fast-XPS) · near-edge X-ray absorption fine structure spectroscopy (NEXAFS)

The on-surface synthesis and assembly of π -electron functional organic molecules has been recently studied extensively, as a potential approach for fabricating novel architectures for use, for example, in nanoelectronic and optoelectronic devices.^{1,2} Self-assembled molecular networks are widely studied in this context; they are characterized by weak supramolecular interactions, exhibiting poor mechanical stability and limited intermolecular charge transport and are thus less compelling systems for technological applications.^{3–7} Connecting molecular building blocks with covalent bonds yields more robust structures, which may be used as active materials in devices. Such single-atom-thick materials

can support efficient charge transport and offer a range of other electronic properties that are actively sought in molecular and nanoelectronics.^{2,8,9}

The synthesis of conjugated polymers in solution is well-established and can be applied on industrial scales, yet it typically yields disordered structures.¹⁰ Improved structural order can be obtained using atomically flat substrates which confine polymer growth to a two-dimensional plane and which also can act as catalysts for the polymerization reaction. The formation of covalent bonds between molecular building blocks on surfaces has been recently reported by several groups, and opens the door to the creation of polymer

* Address correspondence to
duffin@emt.inrs.ca,
dmitrii.perepichka@mcgill.ca,
rosei@emt.inrs.ca,
giorgio.contini@ism.cnr.it.

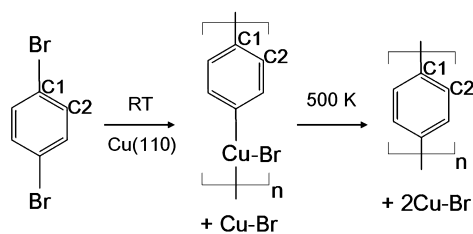
Received for review July 12, 2013
and accepted August 29, 2013.

10.1021/nn4035684

architectures which are impossible to access by standard reactions in solution.^{11–18}

Various methods for obtaining covalently bound π -conjugated structures on surfaces have been successfully demonstrated in air, at the solid–liquid interface and in ultra high vacuum (UHV). On-surface polymerization has been performed in air exploiting the 1,4-addition reaction of diacetylenes, triggered by UV irradiation¹⁹ or by using voltage pulsing from a scanning tunneling microscope (STM) tip,^{20–22} as well as polycondensation of boronic acids upon thermal annealing.²³ At the solid–liquid interface, after pioneering work on diacetylene molecules on graphite,²⁴ pH-controlled Schiff-base formation^{25,26} and electrochemical oxidative coupling^{27,28} have been used to synthesize ordered polyimine and polythiophene monolayers, respectively. In UHV, 2D hybrid ordered superstructures stabilized by supramolecular interactions based on two covalently linked molecular species have been demonstrated.^{29,30} Extended 1D^{31,32} and 2D³³ covalently linked polymers have been produced by thermal treatment of the deposited molecular layers. So far, the most successful approach for obtaining polymers in UHV is the metal-catalyzed coupling of halogen-substituted molecules: this has been widely studied in the past decade,³⁴ exploiting the know-how acquired in the early studies on the adsorption of alkyl- and aryl-halide compounds onto metallic surfaces^{35–38} and their covalent coupling (Ullmann reaction).^{39,40} Structure tailoring of 1D and 2D polymers with desired structure by changing the molecular building blocks^{41,42} has been demonstrated. Following the seminal work reporting dissociative chemisorption of diiodobenzene on copper⁴³ and subsequent formation of phenylene “protopolymer” chains,⁴⁴ ordered covalent 1D conjugated polymers have been realized by using 2,5-diiodo-3,4-ethylenedioxythiophene⁴⁵ and 1,4-diiodobenzene⁴⁶ precursors. Porous graphene and graphene-like 2D polymers have been obtained on metallic surfaces in UHV using Ullmann-like reactions^{47–50} or dehydrogenation.⁵¹ Graphene nanoribbons have been produced using sequential Ullmann and dehydrogenation mechanisms.^{52,53} The conductance properties of a single 1D polymer have been analyzed as a function of its length.⁵⁴

In most of the above studies on surface-confined Ullmann coupling, the occurrence of polymerization was postulated based on local probe measurements only, which have limited chemical sensitivity. The outcome of this reaction has been mainly observed by STM imaging, identifying the distances between molecular units during oligomerization and comparing them with the expected distances obtained from gas phase calculations and by the appearance of new electronic states close to the Fermi level.^{41,55} Moreover, few works focus on the intermediate step of the surface-confined Ullmann reaction^{55–57} and none of them consider the role played by the halogen atom in the organometallic structure.



Scheme 1. Ullmann coupling reaction for 1,4-dibromobenzene on Cu(110).

Using surface-averaged and chemically sensitive techniques, we provide a deeper insight into the intermediate steps of the Ullmann coupling reaction. In particular, we report a spectroscopic study of occupied and unoccupied electronic states at each of the reaction steps and focus on the structural conformation of the organometallic intermediate, which is strongly affected by the choice of halogen. The findings were obtained for a monolayer of ordered poly(*para*-phenylene) (PPP) polymers created by Ullmann coupling of 1,4-dibromobenzene (dBB) on Cu(110) according to Scheme 1, using STM and spectroscopic measurements on the occupied (by X-ray photoelectron spectroscopy, XPS) and unoccupied (by near-edge X-ray absorption fine structure, NEXAFS) electronic states and are supported by first-principles calculations. We also follow in real time the transition from organometallic to polymer phase by fast-XPS, determining the temperature at which the carbon–copper bonds break.

RESULTS AND DISCUSSION

When dBB is deposited on a Cu(110) surface at room temperature (RT), an ordered superstructure is produced, as shown in the STM image in Figure 1a, together with the bare substrate imaged with atomic resolution. Two mirror-symmetric (about $[1\bar{1}0]$) domain orientations were observed (see Figure S1 in Supporting Information). The precursor molecules dehalogenate upon deposition at RT resulting in copper-bound bromine atoms and an organometallic structure, which consists of phenylene groups bonded at each end to Cu atoms. The resulting domains contain nested parallel lines of organometallic chains, which run along the crystalline $[1\bar{1}\bar{1}]$ and $[1\bar{1}1]$ directions and incorporate a strain-relieving single lattice-vector kink at every fourth chain unit. The 2D structure of the domain is created from parallel stacking along the $[1\bar{1}2]$ (or $[\bar{1}12]$) directions.

The organometallic structure obtained at RT is commensurate with the substrate as shown in the low energy electron diffraction (LEED) pattern in Figure 1c, which contains spots originating from two symmetrically equivalent domain orientations. We find an excellent agreement by comparison with a simulated LEED pattern described by the epitaxy matrices $(2, 2 | -4, 9)$ and $(2, -2 | 4, 9)$ that correspond to the unit cells of the two domain orientations observed by STM (see Figure S2 in Supporting Information). The unit cell of the overlayer is highlighted in blue in Figure 1a,b.

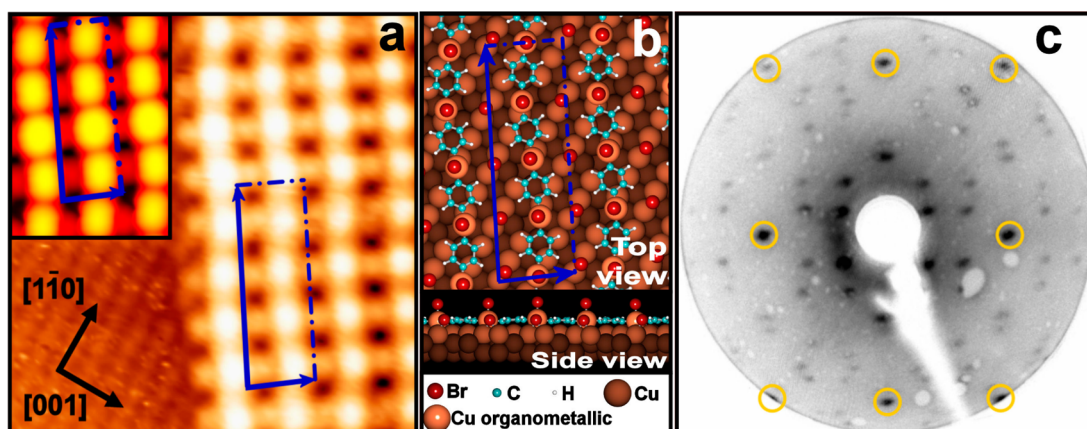


Figure 1. (a) STM image of one domain orientation of a dBB submonolayer on Cu(110) deposited at RT ($5.5 \times 5.5 \text{ nm}^2$, $I_t = 0.77 \text{ nA}$, $V_s = -0.76 \text{ V}$); in the lower left part, copper substrate at atomic resolution is visible; STM simulation for the calculated RT geometry is shown in the inset ($2.1 \times 2.9 \text{ nm}^2$). (b) Top and side views of DFT-optimized RT geometry; atoms are represented as balls according to the legend; unit cell and vectors of the overlayer are shown in blue. (c) Experimental LEED pattern for 1 ML of dBB on Cu(110) at RT ($E_p = 72 \text{ eV}$); circles indicate 1×1 spots.

The measured distance between nearest-neighbor phenylene groups (along the $[1\bar{1}\bar{1}]$ direction, Figure 1a) is $0.62 \pm 0.02 \text{ nm}$, significantly larger than the expected value for PPP (0.433 nm)^{46,58} which implies that the phenylene species are not covalently linked at RT.

The appearance of the RT organometallic structure is both structurally and qualitatively distinct from the RT structure obtained when 1,4-diiodobenzene (dIB) is used as a precursor in similar experiments.⁴⁶ A comparison between the structure arising from using dIB or dBB is shown in Figure 2. The halogens behavior changes in the two cases: iodine from dIB creates $c(2 \times 2)$ islands covering parts of the surface (see blue arrow in Figure 2b), while using bromine the growth of the organometallic phase is allowed over the entire surface, producing extended polymers.

Moreover, the presence of the halogens affects the organometallic structure itself, since the unit cell is different in the two cases, although halogen atoms are detached from the precursor molecules (see below). A model of the RT structure constructed using first-principles density functional theory (DFT) calculations is shown in Figure 1b. It comprises phenylene units and copper atoms that are lifted out of the surface plane and bond the aromatic rings into organometallic chains. The calculated structure has a periodicity of 0.64 nm along the $[1\bar{1}\bar{1}]$ direction, in good agreement with the experimental value. The unit cell contains bromine atoms adsorbed in two distinct environments: four are positioned on the short bridge site of the substrate and four sit on top of the Cu atoms involved in the organometallic structure. This structure is in agreement with the current understanding of the Ullmann reaction mechanism: the organometallic chain corresponds to Ph-Cu-Br-Ph , an expected reaction intermediate and surface-adsorbed bromine corresponds to the expected copper bromide byproduct.⁵⁹ STM simulations for the model provide a much closer qualitative match to the

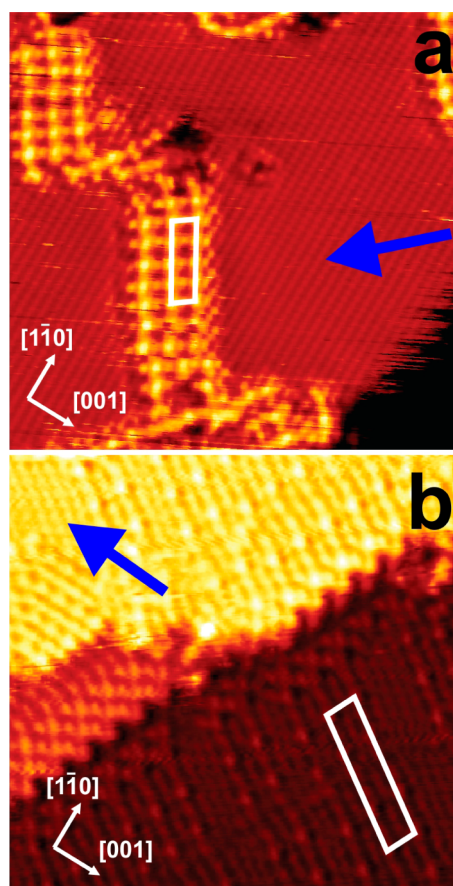


Figure 2. (a) STM image of Cu(110) surface after deposition of dBB at RT ($15.1 \times 14.5 \text{ nm}^2$, $I_t = 0.73 \text{ nA}$, $V_s = -1.16 \text{ V}$); the blue arrow indicates atomic resolution of the substrate. (b) STM image of Cu(110) surface after deposition of dIB at RT ($15.1 \times 14.5 \text{ nm}^2$, $I_t = 0.22 \text{ nA}$, $V_s = -2.05 \text{ V}$); the blue arrow indicates $c(2 \times 2)$ iodine island in between the organometallic structure; white parallelograms indicate the unit cell in the two cases ($(2 \times 2 | -4 \ 9)$ for dBB, $(1 \times 4 | 11 \ 10)$ for dIB).

experimental STM images compared to an identical model without the top Br atoms (Figures 1a and Figure 3).

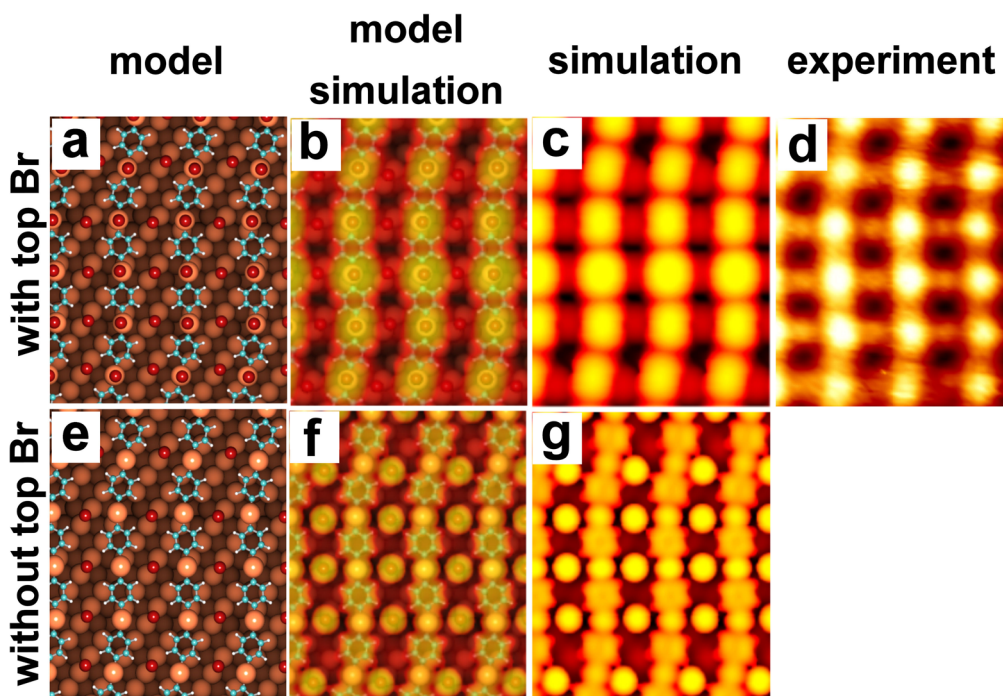


Figure 3. Models (a and e), corresponding STM simulations (c and g), and superposition of the two (b and f) of calculated RT structures with (a–c) and without (e–g) the inclusion of additional Br atoms on top of the Cu atoms in the organometallic chain. The crystallographic orientation and dimensions of all images are identical. Atoms in the models are represented in different colors and sizes according to the legend reported in Figure 1b. Experimental STM image (d) is shown for comparison ($3.2 \times 3.7 \text{ nm}^2$, $I_t = 0.77 \text{ nA}$, $V_s = -0.76 \text{ V}$).

We therefore conclude that the halogen atoms are a critical stabilizing element of the intermediate structure.

XPS analysis of the samples held at low temperature (LT, 100 K), RT and 500 K unequivocally confirm that the dehalogenation is complete at RT, as demonstrated by previous studies,^{36,38} the observed core level shifts are in agreement with those theoretically predicted for bromo- and iodobenzene on different substrates.⁵⁷ The binding energy (BE) shifts of the Br $3d_{5/2}$ core level (Figure 4) reflect the difference between bromine atoms linked to the phenyl ring (at LT, BE = 70.9 eV)⁶⁰ and to the copper substrate (at RT, BE = 68.4 eV and at 500 K, BE = 68.5 eV).⁶¹ The weaker low-BE component of Br 3d at LT is due to damage from the incident beam, which causes dehalogenation (see Figure S3 in Supporting Information). At RT, the weaker high-BE component of Br 3d probably originates from one of the two distinct chemical environments of Br atoms. A comparison of the C 1s spectra collected for dBB deposited at RT and annealed to 500 K with ones at LT on Cu(110) (Figure 4) confirms that the C 1s state at 286.4 eV corresponding to carbon–bromine bonds⁶² vanishes at RT.

Deconvolution of the C 1s core level spectrum of the RT system in Figure 4 supports the interpretation of the RT structure as an organometallic chain: the peak at 283.2 eV is assigned to carbon bound to copper (C1 in Scheme 1), in agreement with the expected lowering of the BE for metal-linked carbon.^{36,38} The other two peaks at 283.8 and 284.2 eV originate from C2 carbons (see Scheme 1) of the dehalogenated molecules; the splitting can be attributed to nonequivalent positions

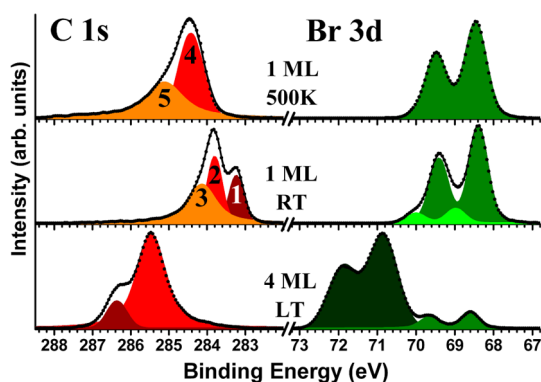


Figure 4. C 1s and Br 3d core level spectra for dBB on Cu(110) deposited at different temperatures: 4 monolayers (ML) deposited at LT, 1 ML deposited at RT and the same surface annealed at 500 K. The spectra are collected using an incident photon energy of 390 eV. Experimental data after Shirley background subtraction⁶³ are shown as points, and fitted Voigt functions are shown as solid filled lines. The numbers identify the fitting functions whose intensities are reported in Figure 7b.

of these carbons in the unit cell and to vibrational broadening of the peak at higher BEs.

Annealing the organometallic structure at 500 K consumes both of the domain orientations observed at RT and yields a new single-domain superstructure aligned along the $[1\bar{1}0]$ direction, shown in the STM image of Figure 5a, which consists of an array of alternating bright and dim lines. The repeat distance is $1.08 \pm 0.02 \text{ nm}$ along the $[001]$ direction, corresponding to $3 \times$ the periodicity of the substrate, consistent with the

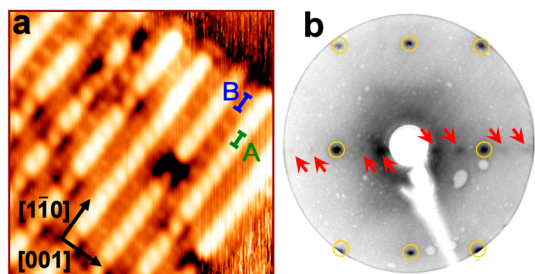


Figure 5. (a) STM image of dBB on Cu(110) after annealing to 500 K for 5 min ($6.8 \times 6.8 \text{ nm}^2$, $I_t = 0.60 \text{ nA}$, $V_s = -0.40 \text{ V}$); the alternating bright and dim lines correspond to rows of PPP and adsorbed bromine, respectively. (b) Experimental LEED pattern for 1 ML of dBB on Cu(110) after annealing at 500 K for 5 min ($E_p = 72 \text{ eV}$); $3 \times$ periodicity along [001] is indicated by red arrows and 1×1 spots by yellow circles.

observed LEED and reflection high energy electron diffraction (RHEED) patterns shown in Figures 5b and S4a in Supporting Information, respectively. The bright lines are interpreted as polymers, since their internal periodicity of $0.44 \pm 0.02 \text{ nm}$ along $[1\bar{1}0]$ (A in Figure 5a) is in agreement with the gas-phase calculated value of 0.433 nm between adjacent rings in poly(*para*-phenylene) (PPP)⁴⁶ or measured in crystal phase for *para*-septiphenyl.⁵⁸ The polymers reach lengths of 20 phenylene units. The dim lines are interpreted as Br atoms arranged in a lattice-commensurate $2 \times$ periodicity since their constituents are spaced by $0.51 \pm 0.02 \text{ nm}$ (B in Figure 5a). These structures match those observed when using dIB as precursor molecule on this surface,⁴⁶ though we note that the differential contrast between the halogen and polymer lines is reversed in our experiments.

The copper-linked carbon contribution at 283.2 eV in the C 1s core level spectrum is not present on the annealed surface (Figure 4). The C 1s signal is shifted toward higher BE and can be deconvoluted into two components at 284.4 and at 285.1 eV which can be assigned to C2 and C1 carbons, respectively (see Scheme 1). These binding energies are in agreement with those observed for *p*-quaterphenyl.⁶² The Br 3d core level spectrum after annealing contains a single doublet, originating from the unique adsorption configuration of Br atoms onto the copper substrate.

While XPS probes changes in the core level electrons, polarization-dependent NEXAFS probes the character of the unoccupied electronic states and is sensitive to long-range bonding and subtle geometrical transformations of organic species. It may be used to confirm the presence of a conjugated structure.⁶⁴ Figure 6 shows two C K-edge NEXAFS spectra for each of the organometallic and polymer phases, collected at $\theta = 90^\circ$ (*p*-polarization) and $\theta = 0^\circ$ (*s*-polarization). The comparison between *p*- and *s*-polarization measurements demonstrate that the phenylene rings in both structures are parallel to the surface (see Supporting Information for details), as predicted by the calculated model.

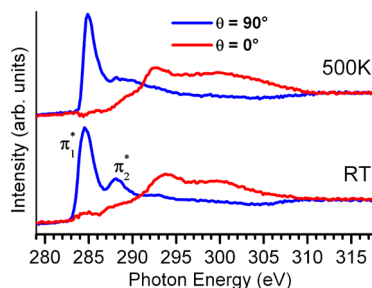


Figure 6. Polarization-dependent C K-edge NEXAFS spectra for the RT (bottom) and annealed (top) samples; two spectra are reported for each sample (refer to Figure S6 in Supporting Information for the definition of the angles): $\theta = 90^\circ$ (blue) and $\theta = 0^\circ$ (red) with the incident radiation falling in the plane containing the sample normal and the [001] lattice direction.

The NEXAFS spectrum obtained from the RT sample using $\theta = 90^\circ$ contains two π^* transitions (labeled π_1^* and π_2^* in Figure 6) at 284.6 and 288.1 eV , in agreement with NEXAFS spectra collected from phenyl adsorbed on Cu(111).⁶⁵ Two π^* resonances are always observed for chemisorbed phenyl rings, its derivatives and heteroanalogues, albeit with different lineshapes and photon energy positions.⁶⁴ In the case of free planar benzene, the NEXAFS spectrum exhibits only one π^* transition; the presence of a second transition at higher photon energy has been attributed to a splitting of the e_{2u} unoccupied state that can be due to a symmetry reduction of the ring caused by geometrical distortions⁶⁶ or to a newly formed state composed of adsorbate π and substrate 3d states.⁶⁷ The calculated structure in Figure 1b indicates that the phenylene rings are distorted from the planar geometry. The presence of a π_2^* resonance is therefore expected at RT.

After annealing to 500 K, π_2^* resonance is strongly suppressed, whereas the π_1^* peak is unaltered in height and becomes narrower in width. The presence of a single resonance in the NEXAFS spectrum is in agreement with reported spectra for *para*-sexiphenyl adsorbed on Cu(110);⁶⁸ thus, the vanishing of the π_2^* state after annealing indicates a return to planarity of each phenylene unit due to the disruption of the organometallic chains and the formation of C–C bonds between adjacent rings. A planar structure is theoretically predicted for the dimerization of phenylene units over Cu(111),⁶⁹ though these calculations neglect the participation of the halogen in the reaction pathway and thus cannot be directly compared to our RT results. Thus, the NEXAFS measurements support the formation of the planar geometry PPP over the majority of the surface.

Fast-XPS spectra at the C 1s core level were recorded during the annealing process from RT to 600 K (Figure 7a), with the aim of following the conversion from organometallic to covalent conjugated polymer. The RT structure remains unchanged until the transition temperature and the polymer structure is stable up to 600 K, since the C 1s line shape does not change.

The reported fast-XPS spectra allow us to dynamically follow the transformation from organometallic to

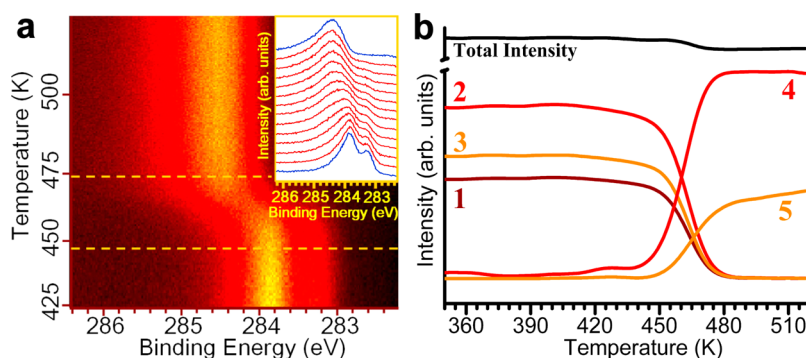


Figure 7. (a) fast-XPS measurement of C 1s core level during annealing, showing the evolution of the spectrum line shape through the transition from organometallic to polymeric phases; the acquisition time for each spectrum is 2 s; the heating rate is 2 K/s; yellow corresponds to higher intensity; the inset shows individual spectra from 443 to 473 K (red curves) stacked as a function of increasing temperature, corresponding to the area in between the yellow dotted lines; the blue curves are the C 1s spectra corresponding to before and after the conversion to polymer. (b) Intensities of the RT and 500 K fitting functions for C 1s core levels, reported as a function of the annealing temperature; numbers and colors identify the peaks as shown in Figure 4.

polymeric phases, measuring the transition temperature for the first time. Figure 7b displays the intensities of the peaks used to fit the C 1s state at RT and 500 K (Figure 4) as a function of temperature. Details of the fitting can be found in Figure S5 in the Supporting Information. The vanishing of the C 1s component corresponding to the carbon–copper bond (curve 1 in Figure 7b), which can be considered the limiting step for the conversion into covalent bonding, gives the transition temperature, which we estimate to be 460 ± 10 K. All the components of the fit present the same transition temperature. During the formation of polymers, the total intensity of C 1s core level signal is reduced by 20%, due to the desorption of molecules induced by annealing.

CONCLUSIONS

We analyzed the organometallic intermediate of the surface-confined Ullmann coupling of 1,4-dibromobenzene precursors on Cu(110), describing its structural

features and establishing that the choice of halogen plays an important role in determining the adsorption conformation. Annealing these structures induces a transition to an extended conjugated polymeric phase, comprising alternating lines of poly(*para*-phenylene) and Br atoms, oriented along the crystal $[1\bar{1}0]$ direction. Spectroscopic insight into this method for obtaining highly controlled and tunable 1D and 2D polymers has been achieved by XPS and NEXAFS measurements. This result is of particular importance, because it represents the first surface-averaged and chemically sensitive spectroscopic signature of this reaction. Specifically, we observed the transition from organometallic into covalent bonding in real-time using fast-XPS, following the process with an acquisition time of 2 s per spectrum and heating rate of 2 K/s. This analysis shows that the bonding conversion temperature is 460 ± 10 K.

METHODS

Experiment. All experiments were performed in UHV chambers with base pressures of 10^{-10} mbar or below. A 110-oriented Cu single crystal was cleaned by repeated cycles of sputtering (Ar^+ , between 600 and 1000 eV) followed by annealing up to 800 K. The precursor 1,4-dibromobenzene (dBB) ($\text{C}_6\text{H}_4\text{Br}_2$, Sigma Aldrich, purity 98%) was dosed into the vacuum chamber *via* a leak valve, using substrates held either at room temperature or cooled to 100 K by liquid nitrogen. Annealing was subsequently performed and the resulting overlayers were analyzed.

STM measurements were performed using a commercial instrument (VT-STM, Omicron Nanotechnology GmbH) housed in a UHV chamber where a LEED apparatus was present (SpectraLEED, Omicron Nanotechnology GmbH). The quoted bias voltages are measured from the tip to the sample. STM images were corrected for drift or piezo artifacts to reflect the known lattice constants of Cu(110), using the free WSxM software.⁷⁰

XPS and NEXAFS spectroscopy measurements were performed on ALOISA beamline⁷¹ at the ELETTRA synchrotron radiation facility (Trieste, Italy), using linearly polarized radiation. RHEED was used to verify the ordering of the molecular superstructures. XPS spectra were obtained in normal emission geometry, using grazing incidence (4 degrees) radiation and a

home-built hemispherical electron analyzer equipped with a multichannel plate (MCP) detector. A Shirley background was subtracted from the core level spectra by using CONTUR software.⁶³ The NEXAFS C K-edge spectra were recorded in partial electron yield mode by means of a channeltron detector, with constant retarding voltages of 240 V between the sample and detector. The drain current on the last refocusing mirror of the beamline was simultaneously acquired for photon energy scale calibration purposes. The spectra were normalized with respect to the signal from the clean Cu(110) surface. Polarization-dependent measurements were performed by rotating the sample about the beam axis, changing the angle (θ) of the polarization vector with respect to the sample surface, while keeping the grazing photon incidence angle fixed at $\alpha = 6^\circ$ (see Figure S6 for the experimental geometry).

Computational Details. DFT calculations were performed using the plane-wave pseudopotential code VASP.^{72,73} We used the generalized gradient (GGA) formulation to approximate the exchange-correlation functional potential proposed by Perdew, Burke and Enzerhof (PBE).⁷⁴ The size of the unit cell was first obtained from the relaxation of a clean Cu(110) surface, resulting in a cell size of $8.842 \times 27.3212 \times 20 \text{ \AA}^3$ ($\gamma = 86.8863^\circ$). The electronic structure calculations were performed using a $8 \times 4 \times 1$ Monkhorst-Pack grid to pave the Brillouin zone.⁷⁵

The pseudopotentials were expressed within the projector augmented wave (PAW) scheme with an energy cutoff of 400 eV.⁷⁶ Once the candidate structures were relaxed within 0.01 eV/Å, the corresponding (constant current) STM images were computed within the Tersoff–Hamann approximation, where the current at a given tip position above the sample is essentially expressed as the integral of the density of states between the Fermi energy and the applied potential.⁷⁷

Conflict of Interest: The authors declare no competing financial interest.

Supporting Information Available: Additional experimental results, NEXAFS experimental geometry, Phenylene ring orientation by NEXAFS. This material is available free of charge via the Internet at <http://pubs.acs.org>.

Acknowledgment. This work was partly supported by NSERC of Canada (Discovery Grants to D.F.P. and F.R.). F.R. is grateful to the Canada Research Chairs program for partial salary support. L.C. is grateful to FRQS for a personal postdoctoral fellowship. D.F.P. and F.R. are grateful to FRONT for team grants. F.R. is grateful to the Alexander von Humboldt Foundation for a F.W. Bessel Award. This work was partially supported by Elsevier through a grant from Applied Surface Science. We acknowledge beamtime access and support from ELETTRA. V.M. is grateful for the support from the Center for Nanophase Materials Sciences (CNMS), sponsored at Oak Ridge National Laboratory by the Division of Scientific User Facilities, U.S. DOE. M.D.G. and G.C. thank Massimo Brolatti for technical assistance during the experiments. J.L.-D., G.C. and M.D.G. are grateful for helpful discussions with Prof. Alessandro Baraldi and Dr. Rosanna Laricprete regarding the treatment of fast-XPS data.

REFERENCES AND NOTES

- Cuevas, J. C.; Scheer, E. *Molecular Electronics—An Introduction to Theory and Experiment*; World Scientific: Singapore, 2010.
- Palma, C.-A.; Samori, P. Blueprinting Macromolecular Electronics. *Nat. Chem.* **2011**, *3*, 431–436.
- Barth, J. V.; Costantini, G.; Kern, K. Engineering Atomic and Molecular Nanostructures at Surfaces. *Nature* **2005**, *437*, 671–679.
- Contini, G.; Gori, P.; Ronci, F.; Zema, N.; Colonna, S.; Aschi, M.; Palma, A.; Turchini, S.; Catone, D.; Cricienti, A.; *et al.* Chirality Transfer from a Single Chiral Molecule to 2D Superstructures in Alaninol on the Cu(100) Surface. *Langmuir* **2011**, *27*, 7410–7418.
- Nath, K. G.; Ivasenko, O.; Miwa, J. A.; Dang, H.; Wuest, J. D.; Nanci, A.; Perepichka, D. F.; Rosei, F. Rational Modulation of the Periodicity in Linear Hydrogen-Bonded Assemblies of Trimesic Acid on Surfaces. *J. Am. Chem. Soc.* **2006**, *128*, 4212–4213.
- MacLeod, J. M.; Ivasenko, O.; Fu, C.; Taerum, T.; Rosei, F.; Perepichka, D. F. Supramolecular Ordering in Oligothiophene–Fullerene Monolayers. *J. Am. Chem. Soc.* **2009**, *131*, 16844–16850.
- Gutzler, R.; Fu, C.; Dadvand, A.; Hua, Y.; MacLeod, J. M.; Rosei, F.; Perepichka, D. F. Halogen Bonds in 2D Supramolecular Self-Assembly of Organic Semiconductors. *Nanoscale* **2012**, *4*, 5965–5971.
- Heath, J. R.; Ratner, M. A. Molecular Electronics. *Phys. Today* **2003**, *56*, 43–49.
- Perepichka, D. F.; Rosei, F. Extending Polymer Conjugation into the Second Dimension. *Science* **2009**, *323*, 216–217.
- Skotheim, T. A.; Reynolds, J. R. *Conjugated Polymers: Theory, Synthesis, Properties, and Characterization*; CRC Press: Boca Raton, FL, 2007.
- Sakamoto, J.; van Heijst, J.; Lukin, O.; Schlüter, A. D. Two-Dimensional Polymers: Just a Dream of Synthetic Chemists? *Angew. Chem., Int. Ed.* **2009**, *48*, 1030–1069.
- Cooper, A. I. Conjugated Microporous Polymers. *Adv. Mater.* **2009**, *21*, 1291–1295.
- Franc, G.; Gourdon, A. Covalent Networks through On-Surface Chemistry in Ultra-High Vacuum: State-of-the-Art and Recent Developments. *Phys. Chem. Chem. Phys.* **2011**, *13*, 14283–14292.
- Méndez, J.; López, M. F.; Martín-Gago, J. A. On-Surface Synthesis of Cyclic Organic Molecules. *Chem. Soc. Rev.* **2011**, *40*, 4578–4590.
- El Garah, M.; MacLeod, J. M.; Rosei, F. Covalently Bonded Networks through Surface-Confined Polymerization. *Surf. Sci.* **2013**, *613*, 6–14.
- Gourdon, A. On-Surface Covalent Coupling in Ultrahigh Vacuum. *Angew. Chem., Int. Ed.* **2008**, *47*, 6950–6953.
- Champness, N. R. Surface Chemistry: Building with Molecules. *Nat. Nanotechnol.* **2007**, *2*, 671–672.
- Bartels, L. Tailoring Molecular Layers at Metal Surfaces. *Nat. Chem.* **2010**, *2*, 87–95.
- Miura, A.; De Feyter, S.; Abdel-Mottaleb, M. M. S.; Gesquière, A.; Grim, P. C. M.; Moessner, G.; Sieffert, M.; Klapper, M.; Müllen, K.; De Schryver, F. C. Light- and STM-Tip-Induced Formation of One-Dimensional and Two-Dimensional Organic Nanostructures. *Langmuir* **2003**, *19*, 6474–6482.
- Okawa, Y.; Aono, M. Materials Science: Nanoscale Control of Chain Polymerization. *Nature* **2001**, *409*, 683–684.
- Okawa, Y.; Aono, M. Nanoscale Wiring by Controlled Chain Polymerization. *Surf. Sci.* **2002**, *514*, 41–47.
- Hla, S.-W.; Bartels, L.; Meyer, G.; Rieder, K.-H. Inducing All Steps of a Chemical Reaction with the Scanning Tunneling Microscope Tip: Towards Single Molecule Engineering. *Phys. Rev. Lett.* **2000**, *85*, 2777–2780.
- Dienstmaier, J. F.; Gigler, A. M.; Goetz, A. J.; Knochel, P.; Bein, T.; Lyapin, A.; Reichmaier, S.; Heckl, W. M.; Lackinger, M. Synthesis of Well-Ordered COF Monolayers: Surface Growth of Nanocrystalline Precursors versus Direct On-Surface Polycondensation. *ACS Nano* **2011**, *5*, 9737–9745.
- Grim, P. C. M.; De Feyter, S.; Gesquière, A.; Vanoppen, P.; Rücker, M.; Valiyaveetil, S.; Moessner, G.; Müllen, K.; De Schryver, F. C. Submolecularly Resolved Polymerization of Diacetylene Molecules on the Graphite Surface Observed with Scanning Tunneling Microscopy. *Angew. Chem., Int. Ed.* **1997**, *36*, 2601–2603.
- Tanoue, R.; Higuchi, R.; Enoki, N.; Miyasato, Y.; Uemura, S.; Kimizuka, N.; Stieg, A. Z.; Gimzewski, J. K.; Kunitake, M. Thermodynamically Controlled Self-Assembly of Covalent Nanoarchitectures in Aqueous Solution. *ACS Nano* **2011**, *5*, 3923–3929.
- Tanoue, R.; Higuchi, R.; Ikebe, K.; Uemura, S.; Kimizuka, N.; Stieg, A. Z.; Gimzewski, J. K.; Kunitake, M. *In Situ* STM Investigation of Aromatic Poly(azomethine) Arrays Constructed by “On-Site” Equilibrium Polymerization. *Langmuir* **2012**, *28*, 13844–13851.
- Sakaguchi, H.; Matsumura, H.; Gong, H.; Abouelwafa, A. M. Direct Visualization of the Formation of Single-Molecule Conjugated Copolymers. *Science* **2005**, *310*, 1002–1006.
- Yau, S.; Lee, Y.; Chang, C.; Fan, L.; Yang, Y.; Dow, W.-P. Structures of Aniline and Polyaniline Molecules Adsorbed on Au(111) Electrode: as Probed by *in Situ* STM, *ex Situ* XPS, and NEXAFS. *J. Phys. Chem. C* **2009**, *113*, 13758–13764.
- Weigelt, S.; Busse, C.; Bombis, C.; Knudsen, M. M.; Gothelf, K. V.; Strunskus, T.; Wöll, C.; Dahlbom, M.; Hammer, B.; Lægsgaard, E.; *et al.* Covalent Interlinking of an Aldehyde and an Amine on a Au(111) Surface in Ultrahigh Vacuum. *Angew. Chem., Int. Ed.* **2007**, *119*, 9387–9390.
- Weigelt, S.; Bombis, C.; Busse, C.; Knudsen, M. M.; Gothelf, K. V.; Lægsgaard, E.; Besenbacher, F.; Linderoth, T. R. Molecular Self-Assembly from Building Blocks Synthesized on a Surface in Ultrahigh Vacuum: Kinetic Control and Topo-Chemical Reactions. *ACS Nano* **2008**, *2*, 651–660.
- Matena, M.; Riehm, T.; Stöhr, M.; Jung, T. A.; Gade, L. H. Transforming Surface Coordination Polymers into Covalent Surface Polymers: Linked Polycondensed Aromatics through Oligomerization of N-Heterocyclic Carbene Intermediates. *Angew. Chem., Int. Ed.* **2008**, *120*, 2448–2451.
- Treier, M.; Richardson, N. V.; Fasel, R. Fabrication of Surface-Supported Low-Dimensional Polyimide Networks. *J. Am. Chem. Soc.* **2008**, *130*, 14054–14055.
- Zwaneveld, N. A. A.; Pawlak, R. M.; Abel, M.; Catalin, D.; Gignes, D.; Bertin, D.; Porte, L. Organized Formation of 2D Extended Covalent Organic Frameworks at Surfaces. *J. Am. Chem. Soc.* **2008**, *130*, 6678–6679.

34. Lackinger, M.; Heckl, W. M. A STM Perspective on Covalent Intermolecular Coupling Reactions on Surfaces. *J. Phys. D: Appl. Phys.* **2011**, *44*, 464011.
35. Solymosi, F. Thermal Stability and Reactions of CH₂, CH₃ and C₂H₂ Species on the Metal Surfaces. *Catal. Today* **1996**, *28*, 193–203.
36. Cabibil, H.; Ihm, H.; White, J. M. The Thermal Chemistry of Iodobenzene on Pt(111). *Surf. Sci.* **2000**, *447*, 91–104.
37. von Schenck, H.; Weissenrieder, J.; Helldén, S.; Åkermark, B.; Göthelid, M. Reactions of Iodobenzene on Pd(111) and Pd(110). *Appl. Surf. Sci.* **2003**, *212–213*, 508–514.
38. Bushell, J.; Carley, A. F.; Coughlin, M.; Davies, P. R.; Edwards, D.; Morgan, D. J.; Parsons, M. The Reactive Chemisorption of Alkyl Iodides at Cu(110) and Ag(111) Surfaces: A Combined STM and XPS Study. *J. Phys. Chem. B* **2005**, *109*, 9556–9566.
39. Ullmann, F.; Bielecki, J. Ueber Synthesen in der Biphenylreihe. *Ber. Dtsch. Chem. Ges.* **1901**, *34*, 2174–2185.
40. Xi, M.; Bent, B. E. Mechanisms of the Ullmann Coupling Reaction in Adsorbed Monolayers. *J. Am. Chem. Soc.* **1993**, *115*, 7426–7433.
41. Grill, L.; Dyer, M.; Lafferentz, L.; Persson, M.; Peters, M. V.; Hecht, S. Nano-Architectures by Covalent Assembly of Molecular Building Blocks. *Nat. Nanotechnol.* **2007**, *2*, 687–691.
42. Lafferentz, L.; Eberhardt, V.; Dri, C.; Africh, C.; Comelli, G.; Esch, F.; Hecht, S.; Grill, L. Controlling On-Surface Polymerization by Hierarchical and Substrate-Directed Growth. *Nat. Chem.* **2012**, *4*, 215–220.
43. McCarty, G. S.; Weiss, P. S. Footprints of a Surface Chemical Reaction: Dissociative Chemisorption of p-Diiodobenzene on Cu(111). *J. Phys. Chem. B* **2002**, *106*, 8005–8008.
44. McCarty, G. S.; Weiss, P. S. Formation and Manipulation of Protopolymer Chains. *J. Am. Chem. Soc.* **2004**, *126*, 16772–16776.
45. Lipton-Duffin, J. A.; Miwa, J. A.; Kondratenko, M.; Ciccoira, F.; Sumpter, B. G.; Meunier, V.; Perepichka, D. F.; Rosei, F. Step-By-Step Growth of Epitaxially Aligned Polythiophene by Surface-Confined Reaction. *Proc. Natl. Acad. Sci. U.S.A.* **2010**, *107*, 11200–11204.
46. Lipton-Duffin, J. A.; Ivashenko, O.; Perepichka, D. F.; Rosei, F. Synthesis of Polyphenylene Molecular Wires by Surface-Confined Polymerization. *Small* **2009**, *5*, 592–597.
47. Gutzler, R.; Walch, H.; Eder, G.; Kloft, S.; Heckl, W. M.; Lackinger, M. Surface Mediated Synthesis of 2D Covalent Organic Frameworks: 1,3,5-Tris(4-bromophenyl)benzene on Graphite(001), Cu(111), and Ag(110). *Chem. Commun.* **2009**, 4456–4458.
48. Blunt, M. O.; Russell, J. C.; Champness, N. R.; Beton, P. H. Templating Molecular Adsorption Using a Covalent Organic Framework. *Chem. Commun.* **2010**, *46*, 7157–7159.
49. Bieri, M.; Nguyen, M.-T.; Gröning, O.; Cai, J.; Treier, M.; Ait-Mansour, K.; Ruffieux, P.; Pignedoli, C. A.; Passerone, D.; Kastler, M.; et al. Two-Dimensional Polymer Formation on Surfaces: Insight into the Roles of Precursor Mobility and Reactivity. *J. Am. Chem. Soc.* **2010**, *132*, 16669–16676.
50. Cardenas, L.; Gutzler, R.; Lipton-Duffin, J.; Fu, C.; Brusso, J. L.; Dinca, L. E.; Vondráček, M.; Fagot-Revurat, Y.; Malterre, D.; Rosei, F.; et al. Synthesis and Electronic Structure of a Two Dimensional π -Conjugated Polythiophene. *Chem. Sci.* **2013**, *4*, 3263–3268.
51. Treier, M.; Pignedoli, C. A.; Laino, T.; Rieger, R.; Müllen, K.; Passerone, D.; Fasel, R. Surface-Assisted Cyclodehydrogenation Provides a Synthetic Route Towards Easily Processable and Chemically Tailored Nanographenes. *Nat. Chem.* **2011**, *3*.
52. Cai, J.; Ruffieux, P.; Jaafar, R.; Bieri, M.; Braunschweig, S.; Muoth, M.; Seitsonen, A. P.; Saleh, M.; Feng, X.; et al. Atomically Precise Bottom-Up Fabrication of Graphene Nanoribbons. *Nature* **2010**, *466*, 470–473.
53. Blankenburg, S.; Cai, J.; Ruffieux, P.; Jaafar, R.; Passerone, D.; Feng, X.; Müllen, K.; Fasel, R.; Pignedoli, C. A. Intraribbon Heterojunction Formation in Ultranarrow Graphene Nanoribbons. *ACS Nano* **2012**, *6*, 2020–2025.
54. Lafferentz, L.; Ample, F.; Yu, H.; Hecht, S.; Joachim, C.; Grill, L. Conductance of a Single Conjugated Polymer as a Continuous Function of Its Length. *Science* **2009**, *323*, 1193–1197.
55. Wang, W.; Shi, X.; Wang, S.; Van Hove, M. A.; Lin, N. Single-Molecule Resolution of an Organometallic Intermediate in a Surface-Supported Ullmann Coupling Reaction. *J. Am. Chem. Soc.* **2011**, *133*, 13264–13267.
56. Blake, M. M.; Nanayakkara, S. U.; Claridge, S. A.; Fernández-Torres, L. C.; Sykes, E. C. H.; Weiss, P. S. Identifying Reactive Intermediates in the Ullmann Coupling Reaction by Scanning Tunneling Microscopy and Spectroscopy. *J. Phys. Chem. A* **2009**, *113*, 13167–13172.
57. Björk, J.; Hanke, F.; Stafström, S. Mechanisms of Halogen-Based Covalent Self-Assembly on Metal Surfaces. *J. Am. Chem. Soc.* **2013**, *135*, 5768–5775.
58. Baker, K. N.; Fratini, A. V.; Resch, T.; Knachel, H. C.; Adams, W. W.; Soggi, E. P.; Farmer, B. L. Crystal Structures, Phase Transitions and Energy Calculations of Poly(p-phenylene) Oligomers. *Polymer* **1993**, *34*, 1571–1587.
59. Sperotto, E.; van Klink, G. P. M.; van Koten, G.; de Vries, J. G. The Mechanism of the Modified Ullmann Reaction. *Dalton Trans.* **2010**, *39*, 10338–10351.
60. Krasnikov, S.; Doyle, C.; Sergeeva, N.; Preobrajenski, A.; Vinogradov, N.; Sergeeva, Y.; Zakharov, A.; Senge, M.; Cafolla, A. Formation of Extended Covalently Bonded Ni Porphyrin Networks on the Au(111) Surface. *Nano Res.* **2011**, *4*, 376–384.
61. Folkesson, B.; Sundberg, P.; Johansson, L.; Larsson, R. An ESCA Investigation of some Copper Complexes. *J. Electron Spectrosc. Relat. Phenom.* **1983**, *32*, 245–256.
62. Beamson, G.; Briggs, D. *High Resolution XPS of Organic Polymers—The Scienta ESCA300 Database*; Wiley: Chichester, 1992.
63. Contini, G.; Turchini, S. CONTUR: A Program for X-Ray Photoemission Spectroscopic Personal Computer-Based Data Analysis. *Comput. Phys. Commun.* **1996**, *94*, 49–52.
64. Stöhr, J. *NEXAFS Spectroscopy*; Springer-Verlag: Berlin, Heidelberg, New York, 2003.
65. Yang, M. X.; Xi, M.; Yuan, H.; Bent, B. E.; Stevens, P.; White, J. M. NEXAFS Studies of Halobenzenes and Phenyl Groups on Cu(111). *Surf. Sci.* **1995**, *341*, 9–18.
66. Pettersson, L. G. M.; Ågren, H.; Luo, Y.; Triguero, L. Benzene Adsorbed on Cu(110): Theoretical X-Ray Absorption, Emission and Shake Calculations. *Surf. Sci.* **1998**, *408*, 1–20.
67. Weinelt, M.; Wassdahl, N.; Wiell, T.; Karis, O.; Hasselström, J.; Bennich, P.; Nilsson, A.; Stöhr, J.; Samant, M. Electronic Structure of Benzene on Ni(100) and Cu(110): An X-Ray-Spectroscopy Study. *Phys. Rev. B* **1998**, *58*, 7351.
68. Novák, J.; Oehzelt, M.; Berkebile, S.; Koini, M.; Ules, T.; Koller, G.; Haber, T.; Resel, R.; Ramsey, M. G. Crystal Growth of Para-Sexiphenyl on Clean and Oxygen Reconstructed Cu(110) Surfaces. *Phys. Chem. Chem. Phys.* **2011**, *13*, 14675–14684.
69. Nguyen, M.-T.; Pignedoli, C. A.; Passerone, D. An *ab Initio* Insight into the Cu(111)-Mediated Ullmann Reaction. *Phys. Chem. Chem. Phys.* **2011**, *13*, 154–160.
70. Horcas, I.; Fernández, R.; Gómez-Rodríguez, J. M.; Colchero, J.; Gómez-Herrero, J.; Baro, A. M. WSXM: A Software for Scanning Probe Microscopy and a Tool for Nanotechnology. *Rev. Sci. Instrum.* **2007**, *78*, 013705–8.
71. Floreano, L.; Naletto, G.; Cvetko, D.; Gotter, R.; Malvezzi, M.; Marassi, L.; Morgante, A.; Santaniello, A.; Verdini, A.; Tommasini, F.; et al. Performance of the Grating-Crystal Monochromator of the ALOISA Beamline at the Elettra Synchrotron. *Rev. Sci. Instrum.* **1999**, *70*, 3855–3864.
72. Kresse, G.; Furthmüller, J. Efficiency of *ab-Initio* Total Energy Calculations for Metals and Semiconductors using a Plane-Wave Basis Set. *Comput. Mater. Sci.* **1996**, *6*, 15–50.
73. Kresse, G.; Furthmüller, J. Efficient Iterative Schemes for *ab Initio* Total-Energy Calculations using a Plane-Wave Basis Set. *Phys. Rev. B* **1996**, *54*, 11169–11186.
74. Perdew, J. P.; Burke, K.; Ernzerhof, M. Generalized Gradient Approximation Made Simple. *Phys. Rev. Lett.* **1996**, *77*, 3865–3868.

75. Monkhorst, H. J.; Pack, J. D. Special Points for Brillouin-Zone Integrations. *Phys. Rev. B* **1976**, *13*, 5188–5192.
76. Blöchl, P. E. Projector Augmented-Wave Method. *Phys. Rev. B* **1994**, *50*, 17953–17979.
77. Tersoff, J.; Hamann, D. R. Theory of the Scanning Tunneling Microscope. *Phys. Rev. B* **1985**, *31*, 805–813.